Effect of magnetic anisotropy on the natural remanent magnetization in the MCU IVe' layer of the Bjerkreim Sokndal Layered Intrusion, Rogaland, Southern Norway

A.R. Biedermann[1,a], M. Jackson[2], D. Bilardello[2], S.A. McEnroe[1]

[1] Department of Geology and Mineral Resources Engineering, Norwegian University of Science and Technology, Sem Sælands vei 1, 7491 Trondheim, Norway
[2] Institute for Rock Magnetism, University of Minnesota – Twin Cities, 100 Union St SE, MN 55455 Minneapolis, USA
[a] Now at: Institute for Rock Magnetism, University of Minnesota – Twin Cities, 100 Union St SE, MN 55455 Minneapolis, USA

Corresponding author: Andrea R. Biedermann (andrea.regina.biedermann@gmail.com)

Key Points:

- Orientation of magnetic fabric and NRM direction change along layer

- NRM appears to be deflected away from paleofield and towards maximum susceptibility

- No correlation between NRM intensity and fabric orientation

The final version of this article is available on the JGR website:

http://onlinelibrary.wiley.com/doi/10.1002/2016JB013506/full

Abstract

A strong negative magnetic anomaly, caused by an intense natural remanent magnetization (NRM) ca. opposite today's geomagnetic field, is observed above the MCU IVe' unit of the Bjerkreim Sokndal layered intrusion. The anomaly is strongest in the east, close to Heskestad, and decreases when following the layer towards the north and west. This study investigates how the NRM changes along the layer, and how its direction and intensity are affected by magnetic fabrics in the intrusion. NRM, low-field anisotropy of magnetic susceptibility and anisotropy of anhysteretic remanence have been measured on 371 specimens from 46 sites. The orientation of both the magnetic fabrics and the NRM change for different locations along the layer, and it appears that the NRM is tilted away from the mean paleofield and towards the direction of maximum susceptibility and maximum anhysteretic remanence. When NRM directions are corrected for magnetic fabrics, the angle between the NRM and mean paleofield direction generally decreases for specimens with a single-component NRM. No correlation was found between the NRM intensity and the directional relationship between NRM, magnetic fabric and mean paleofield.

1 Introduction

The Bjerkreim Soknad Layered Intrusion (BKS) in Rogaland, Southern Norway, is associated with a sequence of positive and negative magnetic anomalies [*McEnroe et al.*, 2009a; *McEnroe et al.*, 1996; *McEnroe et al.*, 2001b]. The most prominent negative anomaly is observed above a particular layer, MCU IVe', of the intrusion. It is strongest near Heskestad, in the east of the intrusion, where the magnetic field is 13,000 nT below background at an elevation of 45 m above ground, and becomes weaker to the north and west [*McEnroe et al.*, 2004a; *McEnroe et al.*, 2004b]. This anomaly is caused by strong natural remanent magnetization of up to 60 A/m, which was acquired ~916 Ma ago, in a field approximately opposite to today's magnetic field, with a mean direction of D = 303.4°, I = -73.5° [*Brown and McEnroe*, 2015]. The NRM has been described as arising from lamellar magnetism in hemo-ilmenite, i.e. ilmenite with hematite exsolution lamellae [*McEnroe et al.*, 2009a; *McEnroe et al.*, 2001b]. It is carried in the contact layers between hematite lamellae and ilmenite host, which formed by diffusion processes during slow cooling of the BKS, and is characterized by large intensity, high coercivity and high thermal stability [*Nabi and Pentcheva*, 2010; *Pentcheva and Nabi*, 2008; *Robinson et al.*, 2002; 2004]. The saturation magnetization of hemo-ilmenite, if all contact layers are magnetized in-phase, is 55 kA/m (cf. magnetite: 480 kA/m, hematite 2.5 kA/m), and lamellar magnetism can thus account for a saturation magnetization of ca. 30 A/m in a rock containing 1% hemo-ilmenite if 6% of the contact layers are in-phase [*Robinson et al.*, 2002].

Hemo-ilmenite occurs in the BKS intrusion both as individual grains or as exsolutions within pyroxenes. In addition, magnetite is present in most layers, including the MCU IVe' unit. *McEnroe et al.* [2004a] and *McEnroe et al.* [2009b] explain the strong negative anomaly in Heskestad by (1) strong preferred orientation of pyroxenes containing oriented hemo-ilmenite exsolutions in favorable orientation with respect to the paleofield, and (2) induced magnetization in magnetite from the local stray field of the hemo-ilmenite NRM. Lamellar magnetism in hemo-ilmenite and ilmeno-hematite has been reported in other areas on Earth, e.g. metamorphic rocks in S Norway, granulite rocks in SW Sweden, the Adirondack Mountains in the US, and Allard Lake, Canada, and may explain the remanent magnetization on Mars [*Brown and McEnroe*, 2012; *McEnroe and Brown*, 2000; *McEnroe et al.*, 2007a; *McEnroe et al.*, 2002; *McEnroe et al.*, 2009b; *McEnroe et al.*, 2001a; *McEnroe et al.*, 2007b; *McEnroe et al.*, 2016].

The magnetic properties of hemo-ilmenite are strongly anisotropic, with the minimum susceptibility normal to the basal plane [*Hargraves*, 1959; *Robinson et al.*, 2013; *Robinson et al.*, 2006]. Both *Hargraves* [1959] and *Robinson et al.* [2006] found that the NRM of hemo-ilmenite is confined to the basal plane, at an angle of at least 80° from the minimum susceptibility axis, in agreement with predictions from lamellar magnetism theory. A recent study by *Robinson et al.* [2013] reports that the NRM in hemo-ilmenite samples from Allard Lake is deflected from the Proterozoic magnetizing field as a result of being confined to the basal plane of hemo-ilmenite. They also show how the NRM intensity is expected to vary with the angle between the preferred hemo-ilmenite orientation and the geomagnetic field at the time the rocks were magnetized, and compare it to measurements on massive hemo-ilmenite ore deposits from Allard Lake. Because the magnetic anomaly over MCU IVe' in the BKS is largely caused by remanent magnetization, a change in the strength of the anomaly indicates a change in NRM intensity and/or direction. Other than the abundance of oxides, which directly affects NRM intensity, this may be due to the strong anisotropy, in combination with a preferred orientation of hemo-ilmenite at different locations in the layer.

Rocks from layered intrusions often have strong petrofabrics and this may result in anisotropy of magnetic properties, both susceptibility and remanence [e.g. *O'Driscoll et al.*, 2015]. For example, anisotropy of magnetic susceptibility has been described in the Skaergaard layered intrusion [*Girdler*, 1961], the Bushveld Complex [*Feinberg et al.*, 2006; *Ferré et al.*, 1999], Rum Layered Suite, NW Scotland [*O'Driscoll et al.*, 2007], the Insizwa layered mafic intrusion, South Africa [*Ferré et al.*, 2002], the Sonju Lake layered intrusion, NE Minnesota [*Maes et al.*, 2007], and the Clearwater Complex, Canada [*Halls and Hanes*, 1999]. Anisotropy of remanence has been reported in the Stillwater Complex [*Selkin et al.*, 2000]. Anisotropy of susceptibility and anisotropy of remanent magnetization have recently been characterized for the cumulate series of the BKS intrusion [*Biedermann et al.*, 2016].

It has been long recognized that magnetization directions can be affected by anisotropy, either (1) due to anisotropic NRM acquisition in a material with a strong pre-existing fabric, or (2) by compaction or deformation after NRM acquisition, causing both fabric development and NRM reorientation. *King* [1955] observed NRM deflection in artificially deposited sediments and defined a relationship between the observed inclination (I_0) and the field inclination (I_f), $\tan(I_0) = f \tan(I_f)$, where f is the flattening factor. A similar function was described for synthetic sediments by *Anson and Kodama* [1987]. Early studies on NRM deflection in natural samples describe NRMs within or near the easy planes of hematite in a hemo-ilmenite ore deposit [*Hargraves*, 1959], and within the cleavage plane, which corresponds to the plane of highest susceptibility, in Welsh slates [*Fuller*, 1960; 1963]. Systematic and significant deviations of TRM from the direction of the magnetizing field have been reported, particularly in well-foliated, magnetically anisotropic rocks [*Uyeda et al.*, 1963]. Further, it has been shown that NRM deflections can correlate with strain [*Cogné and Perroud*, 1988; *Kligfield et al.*, 1983; *Lowrie et al.*, 1986]. NRM deflections have since been described in many synthetic and natural rock types with different mineralogy [*Bressler and Elston*, 1980; *Huang et al.*, 2015; *Lovlie and Torsvik*, 1984; *Tan and Kodama*, 2002; *Tarduno*, 1990; *Tauxe and Kent*, 1984]. This effect may have severe consequences for paleomagnetic interpretations. For example, shallow paleomagnetic directions can lead to the interpretation that a rock was magnetized at lower latitudes, however, they can also be caused by anisotropy-induced deflection of a steeper NRM, with major influence on apparent polar wander paths and paleogeographic reconstructions [*Bilardello and Kodama*, 2010a; *Krijgsman and Tauxe*, 2004; *Muttoni et al.*, 2003; *Tan and Kodama*, 1998; *Vaughn et al.*, 2005]. For this reason, some authors warn against using paleomagnetic data from anisotropic rocks [*Kirker and McClelland*, 1997].

Anisotropy also affects the intensity of the magnetization, which is largest when the magnetizing field was parallel to the easy magnetization axis or plane. *Hargraves* [1959] showed decreasing NRM intensity with increasing angle between the plane of maximum susceptibility and the magnetizing field in hemo-ilmenite ore deposits at Allard Lake. Similar observations have been made both in natural samples and in experiment, and may influence paleointensity and archeointensity studies [*Aitken et al.*, 1981; *Rogers et al.*, 1979]. *Selkin et al.* [2000] imparted laboratory TRMs on anorthosite samples from the Stillwater Complex in different orientations, and found that the TRM intensity varies by more than a factor of 2.5.

A number of methods have been proposed to account for the effects of anisotropy, e.g. based on the flattening functions of *King* [1955]. *Aitken et al.* [1981] proposed to minimize the anisotropy effect by applying the laboratory TRM in the same direction as the NRM, which would be pertinent for paleointensity determinations. This requires, however, that specimens can be oriented during heating, and that the NRM consists of a single component of magnetization. A different approach is to use magnetic anisotropy to correct for NRM deflections [*Lowrie et al.*, 1986]. Low-field anisotropy of susceptibility probes all minerals in a rock, and can have a different magnetic fabric from the remanence-carrying minerals [*Stephenson et al.*, 1986]. *Jackson et al.* [1991] corrected NRM deflections in sediments by multiplying the measured DRM with the inverse of the anisotropy of remanence tensor, adjusted for the anisotropy of the individual remanence-carrying particles. Observed flattening factors alone should not be used to correct NRM directions, because they vary with lithology and over broad ranges [*Bilardello and Kodama*, 2010a; b; *Tauxe et al.*, 2008, and references therein]. Therefore, one would ideally determine which mineral(s) carry the NRM, and then correct the NRM directions with the remanence anisotropy tensor of the same mineral(s). *Tauxe and Kent* [2004] alternatively proposed the elongation/inclination statistical technique, which requires a large amount of paleomagnetic data in addition to reliable models of the geomagnetic field.

The aim of this study is (1) to determine NRM and magnetic anisotropy in the MCU IVe' layer of the Bjerkreim Sokndal Layered Intrusion, as well as other sites within the intrusion that possess a steeply negative NRM, (2) to investigate how NRM directions are affected by magnetic fabrics, and (3) to determine whether the directional relationship between paleofield and magnetic fabric had an influence on the NRM intensity. To achieve this, observed NRM directions are compared to low-field anisotropy of magnetic susceptibility (AMS) and anisotropy of anhysteretic remanent magnetization (AARM).

2 Geological Setting

The Late Proterozoic BKS layered intrusion is part of the Rogaland Anorthosite Province (RAP), which forms the Southern end of the Sveconorwegian orogenic belt. The RAP contains three massif-type anorthosites generated from a basaltic magma, the BKS intrusion and a series of dykes originating from jotunitic parental magma. The layered intrusion covers 230 km^2, contains up to 7 km of cumulate minerals, overlain by acidic rocks, and was emplaced over a short time period 931±2 Ma ago. The cumulate series consists of several megacyclic units (MCUIa, MCUIb, MCUII, MCUIII, MCUIV), each representing an influx of new primitive magma and containing several layers due to fractional crystallization. Ilmenite was an early liquidus mineral, and oxides segregated and were concentrated during high-temperature subsolidus deformation, so that the RAP hosts Fe-Ti-deposits of economic interest [*Duchesne*, 1972; 1999; 2001; *Karlsen et al.*, 1996; *Korneliussen et al.*, 2000; *Michot*, 1960; 1965; *Robins and Wilson*, 2001; *Schärer et al.*, 1996; *Wilson et al.*, 1996]. The layer of main focus in this study, MCUIVe consists of plagioclase, orthopyroxene, clinopyroxene, hemo-ilmenite, magnetite and apatite. Thus it contains two types of iron oxide minerals, magnetite and hemo-ilmenite. Both of these can occur either as individual grains or as exsolutions within pyroxenes. Minor element chemistry of the iron oxides and its relation to magnetic properties has been described by *Robinson et al.* [2001].

The rocks in the Bjerkreim lobe of the BKS follow a syncline structure [*Paludan et al.*, 1994]. Strong foliation has been reported on the limbs of the syncline, and a lineation-dominated fabric caused by the superposition of an initial magmatic layering and a tectonic overprint in the hinge zone. Magnetic fabrics, as defined by anisotropy of susceptibility and anisotropy of remanence, are strong in the entire intrusion and broadly reflect the orientation of the layering [*Biedermann et al.*, 2016; *Bolle et al.*, 2000; *Paludan et al.*, 1994]. The folding has been interpreted as a syn- to post-magmatic event caused by gravitational instability related to the emplacement of the surrounding anorthosite bodies at 930 Ma [*Bolle et al.*, 2000]. *Bolle et al.* [2002] estimate the deformation temperature of the BKS cumulate series to 900 ^{o}C, based on a geothermometry study on the Egersund-Ogna anorthosite [*Maquil and Duchesne*, 1984]. It is thus a solid-state deformation, which took place before the rocks were magnetized. The temperature at which hemo-ilmenite lamellae exsolve and get magnetized is slightly lower than 520 ^{o}C, and the magnetite blocking temperature is between 550 ^{o}C to 570 ^{o}C, leading to a magnetization age of 916 Ma [*Brown and McEnroe*, 2015], i.e. the NRM was acquired post-folding. Similar paleofield directions are reported for the BKS intrusion, D = 303.4^{o}, I = -73.5^{o}, α_{95} = 3.7^{o} [*Brown and McEnroe*, 2015], and one of the surrounding anorthosites, the Egersund-Ogna anorthosite, which was magnetized ca. 900 Ma ago, with D = 325.9^{o}, I = -80.1^{o}, α_{95} = 4.9^{o} [*Brown and McEnroe*, 2004].

3 Materials and Methods

3.1 Sample Description

Oriented samples were collected in the magnetic low associated with the MCU IVe' layer of the BKS. The anomaly related to the MCU IVe' layer is strong and well-defined in the eastern part of the intrusion, but becomes weaker and thus more difficult to identify towards the northern and western parts. Therefore, other samples with negative remanence, but originating from other layers and associated with smaller negative anomalies are also included for the northern and western parts of the intrusion. Additional specimens were available from earlier studies [*Brown and McEnroe*, 2015]. Newly collected specimens are labelled BK2015_xx, and specimens available from earlier studies are named BKxx. The magnetic fabrics of some of these specimens have been described previously [*Biedermann et al.*, 2016]. In total, 371 specimens from 46 sites, including 265 new specimens from 95 drill cores in 29 sites, and 106 existing specimens from 16 drill cores and 13 oriented blocks in 17 sites, were selected for this study (Figure 1). Strong magnetic anomalies affect compass readings. Therefore, the known direction to a far-away point, e.g. the sun or a mountain peak a long distance away, was measured in addition to the sample orientation for each drill core. Sun corrections were preferred but not always possible due to inclement weather. Based on this, 72 sample orientations have been adjusted.

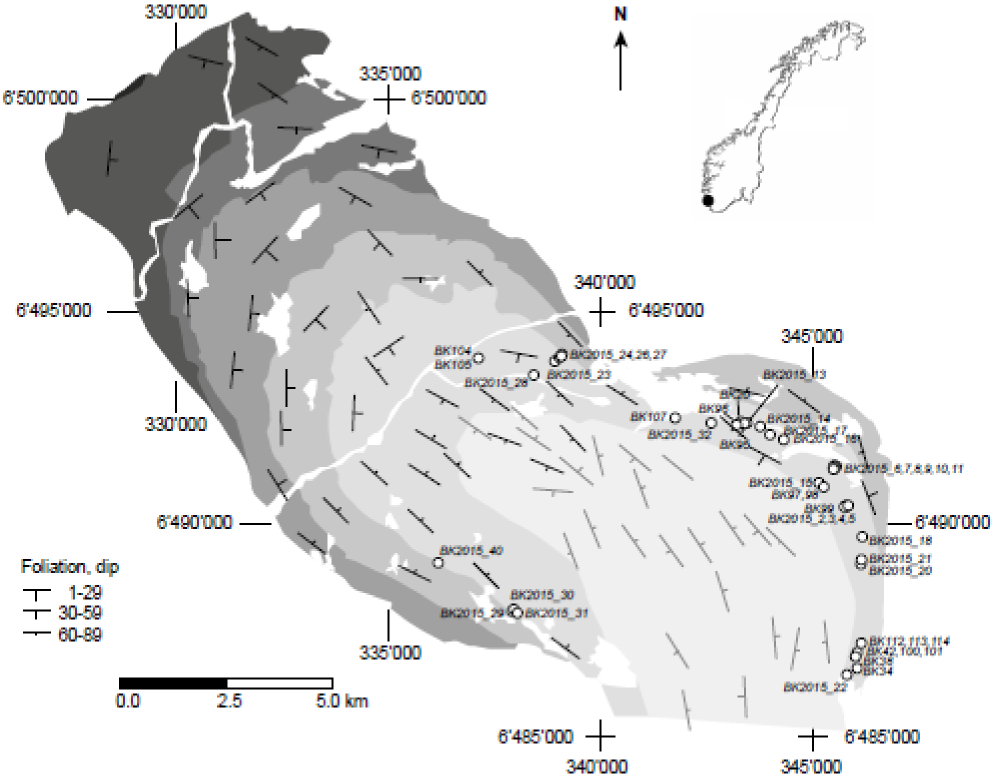

***Figure 1**: Simplified geological map of the BKS and site locations, including macroscopic foliations from Paludan et al. [1994] – black, and magnetic foliation from Bolle et al. [2000] – grey. Note that due to the strong magnetic anomalies, and need of correcting compass readings, the foliation directions may not be accurate in the east and northeast of the BKS. Coordinate system UTM32N, redrawn after McEnroe et al. [2009a]. Inset shows the geographic location of the intrusion in Norway.*

3.2 Natural remanent magnetization

The BK sample collection had been measured on an Agico (Brno, Czech Republic) JR-6 spinner magnetometer or a 2G cryogenic magnetometer at the Norwegian Geological Survey (NGU) and the University of Massachusetts [*Brown and McEnroe*, 2015]. The NRM of some samples was too strong for the cryogenic magnetometer and only small pieces could be measured. The NRM of all BK2015 specimens was measured on an Agico JR-6A spinner magnetometer at NGU. Specimens were rotated in three mutually perpendicular planes to determine the intensity and direction of the NRM. Site means were calculated for all sites, and the reliability of the site mean is assessed by the precision parameter κ and the confidence angle α_{95}. On one specimen of each site, the stability of the NRM was tested by alternating field (AF) demagnetization, using an Agico LDA5 demagnetizer at the Norwegian University of Science and Technology. Specimens were demagnetized at 10 mT increments up to 100 mT or 160 mT, followed by 20 mT increments up to a maximum field of 200 mT.

3.3 Magnetic anisotropy

Magnetic fabrics can be described by the anisotropy of susceptibility or the anisotropy of remanent magnetization. Low-field AMS was initially measured on an Agico MFK1-FA susceptibility bridge at Uppsala University, and later on an MFK1-A susceptibility bridge at the Norwegian University of Science and Technology. Measurements were performed on all specimens, in a field of 200 A/m and at a frequency of 976 Hz, which are the standard field and frequency of the MFK instruments. The magnetic susceptibility tensor was calculated from measurements in the spinning specimen mode or the manual 15-orientations scheme [*Jelinek*, 1977; 1996]. The difference between results obtained with these two methods is less than 1 %, and the two instruments also give virtually the same results. On eight samples, AMS has been measured before any treatment, and after AF demagnetization to 100 mT and 200 mT, which gave the same results for AMS principal directions and anisotropy parameters.

Low-field AMS is described by the eigenvalues, i.e. principal susceptibilities $k_1 \geq k_2 \geq k_3$, and the corresponding eigenvectors of the susceptibility tensor. It can be further characterized by the degree and shape of the anisotropy, and the following parameters will be used throughout this study:

$P = k_1/k_3$,

$k' = \sqrt{[(k_1 - k_{mean})^2 + (k_2 - k_{mean})^2 + (k_3 - k_{mean})^2]/3}$, where $k_{mean} = (k_1 + k_2 + k_3)/3$ is the mean susceptibility, and

$U = (2k_2 - k_1 - k_3)/(k_1 - k_3)$ [*Jelinek*, 1981; 1984].

Anisotropy of anhysteretic remanence (AARM) was measured on a selection of 63 specimens from the 29 new sites and 1 specimen from the existing collection, at the Institute for Rock Magnetism, University of Minnesota. Prior to imparting any remanence, the magnetization remaining after AF demagnetization to 200 mT was measured, and later removed as a background signal. To impart anhysteretic remanence (ARM), DC bias fields of 0.1 mT were applied during AF decay between 100 mT – 0 mT in a DTech D-2000 Precision Instruments AF demagnetizer. The ARM was measured for each orientation with a 2G Enterprises (Mtn. View, CA, USA) RF SQUID superconducting rock magnetometer (SRM). Initially, the ARM was applied and measured in 9 directions per specimen. This measurement scheme was later replaced by a 3-position measurement, because the AARM calculated from the full-vector measurement in 3 orientations was indistinguishable from the AARM calculated from the parallel-components of the 9 measurements. The AARM is described by the same parameters as the low-field AMS.

4 Results

4.1 Natural remanent magnetization

The NRM intensity varies from 0.3 to 60 A/m (Table S1, Supporting Information). The highest intensities are observed in site BK112, close to Heskestad. NRM orientations are generally well grouped within sites, and steeply negative, with site mean inclinations ranging between -43° and -86° (in geographic coordinates). The declination broadly shows a systematic change with geographic location (Figure 2, Table 1). Seven sites (BK2015_8, _10, _11, _15, _26, _30 and _40) display 95% confidence angles (α_{95}) larger than 10° and are excluded from further consideration. Site BK2015_26 shows a bimodal distribution of NRM intensities and directions. The 95% confidence angles of the other sites vary between 1.7° and 9.9°, with a median confidence angle of 6.3°.

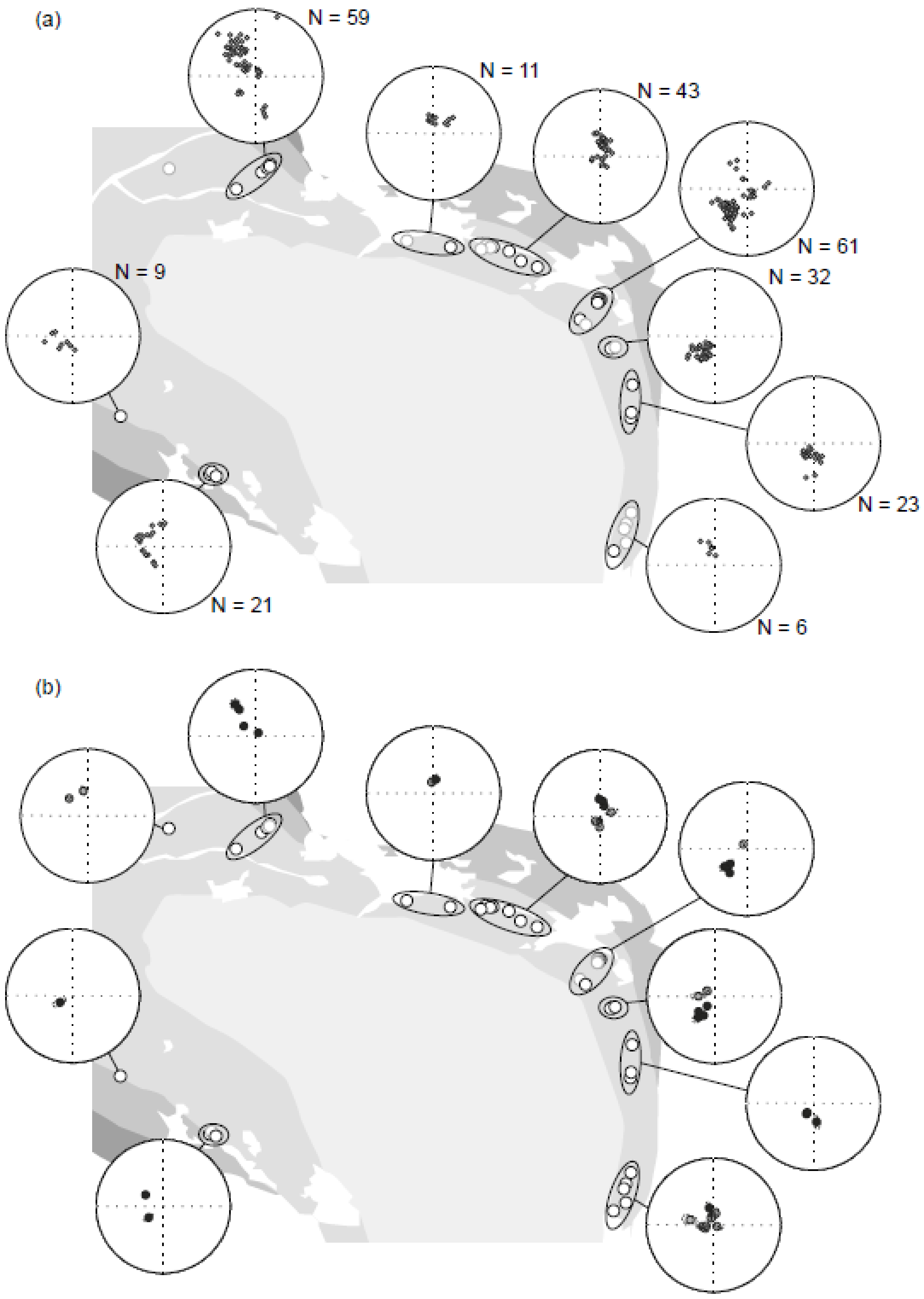

***Figure 2: (a)** NRM directions of individual specimens, BK2015 sample collection, **(b)** site means (black); dotted line: α_{95} confidence circle) of sites with α_{95} < 10°. Site mean demagnetized NRM directions are plotted for specimens from a previous study (Brown & McEnroe, 2015) for comparison (grey). All the NRMs plot in the upper hemisphere, and the stereonets are oriented such that N is at the top of the page, in accordance with the map (cf. Figure S1, Supporting Information for individual plots per site). Sites are marked with grey circles when no data was available or when results have been excluded due to low confidence in this and subsequent figures.*

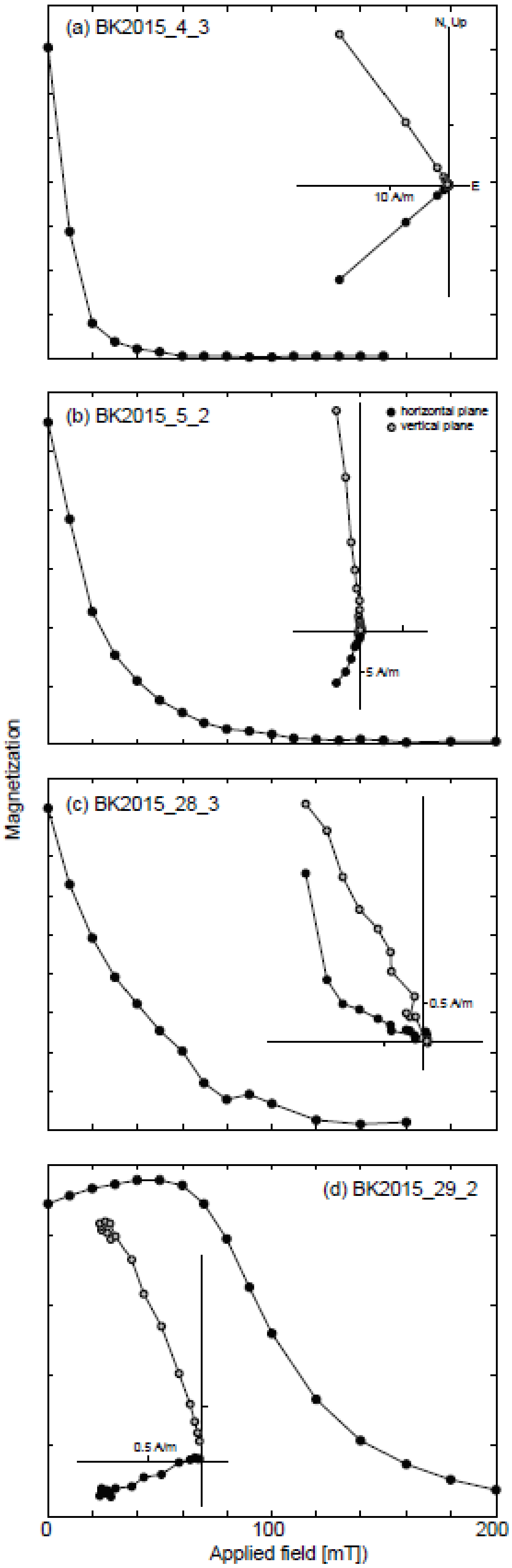

Figure 3: *Typical AF demagnetization behaviors, geographic coordinate system. Insets showing Zijderveld plots to illustrate behavior of NRM directions during AF demagnetization.*

AF demagnetization shows two behaviors for specimens from the MCU IVe' layer; ~90 % of the NRM is removed by 20-30 mT in one group, or by 60 mT in a second group (Figure 3), which both comprise what we refer to here as the low-coercivity component. Specimens from outside MCU IVe' commonly display higher coercivities and lower remanence. Specimens mainly from the eastern part of the intrusion do not show any significant change in NRM directions during demagnetization (sites BK2015_2 to _7, _9, _14, _18, _20, _21). In contrast, changes of directions are observed in specimens from the northern or western parts (BK2015_17, _24, _27 to _29, _31), indicating several components of magnetization with different orientations, even though the initial NRM is steeply negative. For these sites, we report both the NRM and characteristic remanence (ChRM) directions in Table 1. Part of the NRM (up to 10 % of the initial NRM) cannot be removed by AF demagnetization up to 200 mT.

4.2 Magnetic susceptibility and anisotropy

Mean susceptibility varies from $9.4*10^{-4}$ to $2.2*10^{-1}$ (SI) (Table S1, site means cf Table 1). Low-field AMS is significant in all 371 specimens. The degree of anisotropy is high, with P ranging from 1.09 to 2.71, and k' between $8.7*10^{-5}$ and $8.8*10^{-2}$, or 3.6 to 40.7 % of the mean susceptibility. Most specimens exhibit an AMS ellipsoid with a prolate shape, but U varies over the entire range of shapes, between -0.92 and 0.75.

Principal susceptibility directions are well grouped in the majority of sites (Figure 4; note that principal orientations are plotted on the upper hemisphere, counter to convention, to facilitate comparison with NRM orientations). Site means were calculated for the 40 sites with ≥ 5 specimens, the minimum required for *Jelinek* [1981] statistics, and are reported together with their confidence ellipses. In two sites (BK2015_13, _15), only the maximum susceptibility axis is well-defined, whereas the intermediate and minimum susceptibility axes form a girdle, as can be seen from their confidence angles > 30°. Scattered directions are observed in one site, BK2015_10, for which all three principal axes have one confidence angle > 40°. The low-field AMS of this site will not be discussed further. Interestingly, AMS principal directions are consistent for all specimens of site BK2015_26 which displays a bimodal distribution for NRM intensity and directions.

The orientation of the site-mean principal susceptibility axes is generally similar in sites that are located close together, but changes in accordance with the trend of the layers. Overall, the minimum susceptibility is approximately perpendicular to the foliation and magmatic layering, as has been found on a subset of specimens previously studied [*Biedermann et al.*, 2016; *Paludan et al.*, 1994].

4.3 Anisotropy of remanence

Anisotropy of anhysteretic remanence is significant in all but five of the 63 specimens on which it was measured (Table S2, Supporting Information). None of the specimens measured for site BK2015_29 possesses an AARM, and in sites BK2015_7, BK2015_27 and BK2015_40, the AARM may or may not be significant. The mean anhysteretic remanence varies between $1.5*10^{-6}$ Am^2/kg and $7.5*10^{-5}$ Am^2/kg ($4.3*10^{-3}$ A/m – 0.24 A/m) . The degree of anisotropy is generally higher than for AMS; P varies from 1.26 to 3.62, and k' from $2.1*10^{-7}$ to $2.9*10^{-5}$ Am^2/kg, or 11.1 % to 53.7 % of the mean anhysteretic remanence, respectively. The shape of the remanence ellipsoid is dominantly prolate, and varies from U = -0.91 to 0.30.

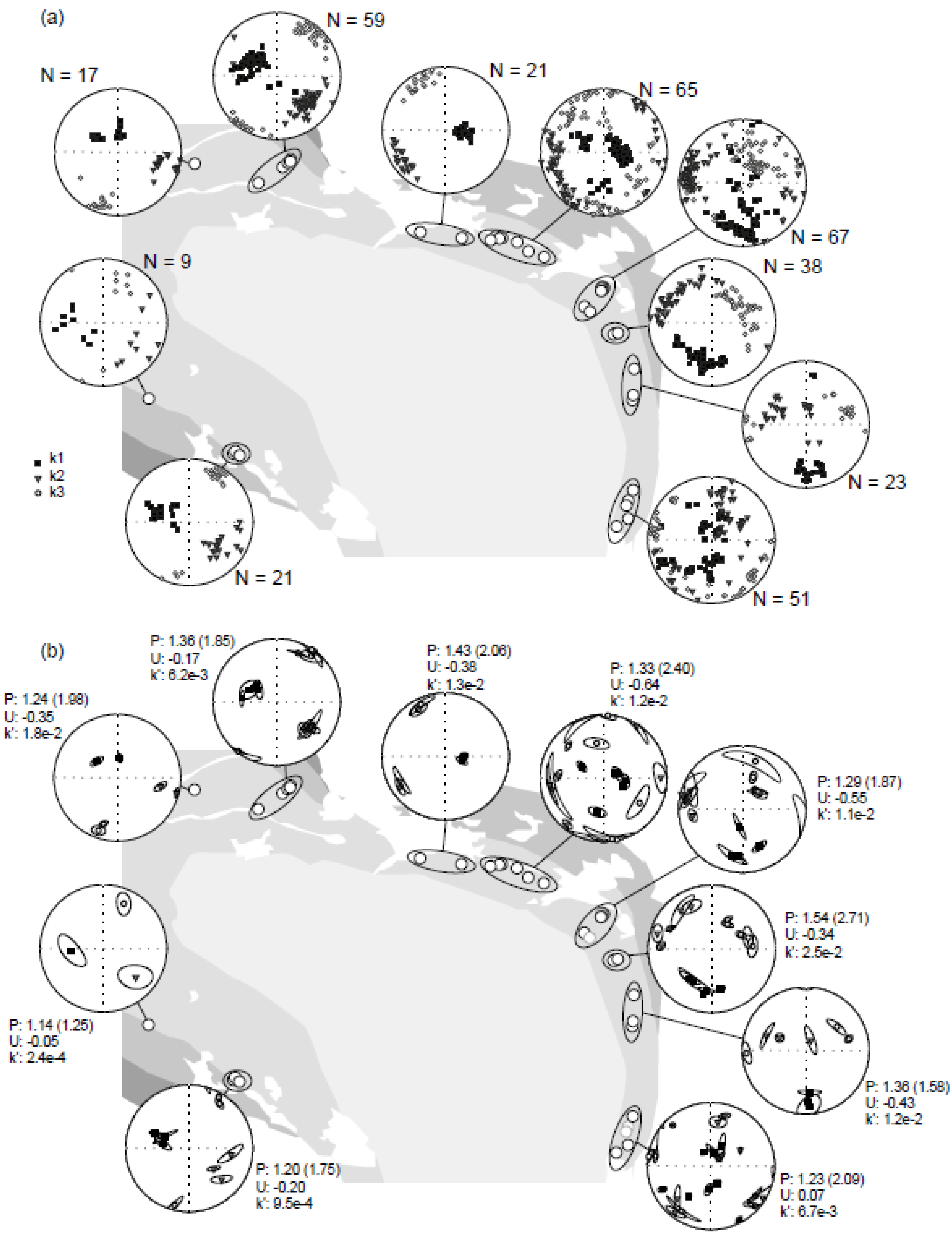

***Figure 4: (a)** AMS for individual specimens and **(b)** AMS site means and confidence ellipses. Square – maximum susceptibility; triangle – intermediate susceptibility; circle – minimum susceptibility. Equal-area stereoplots of the upper hemisphere for direct comparison with the upward pointing NRM. P, U and k' of the mean normalized tensor, as well as the maximum P-value for each group of sites is given next to the stereoplots.*

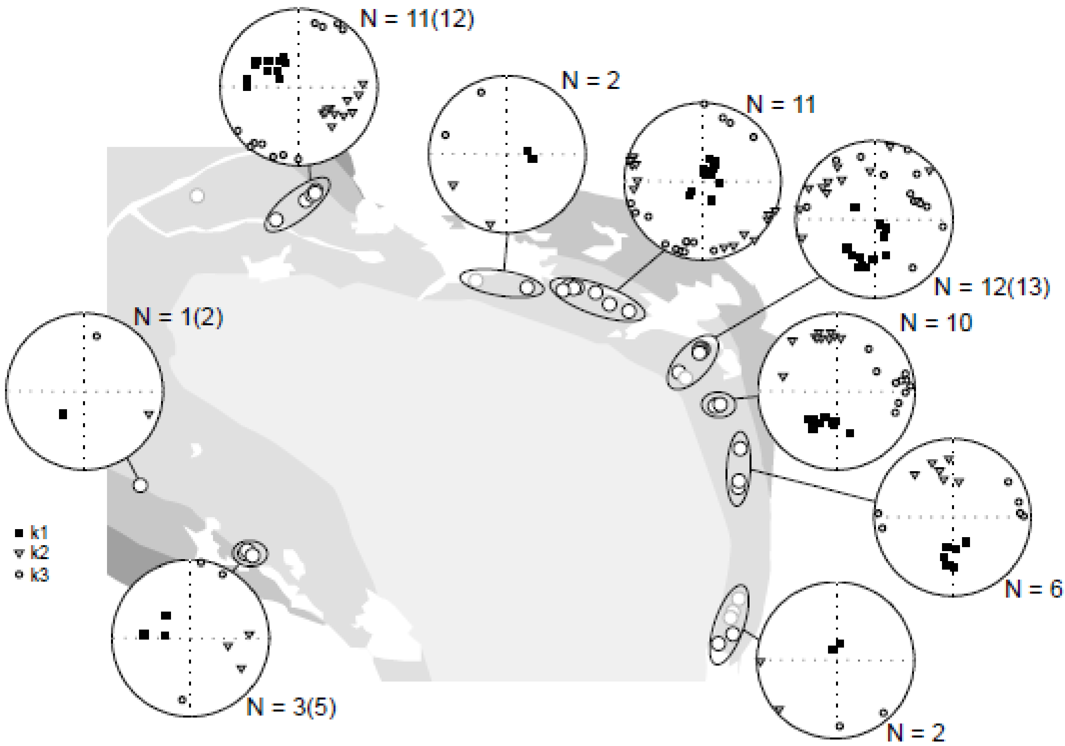

Figure 5*: AARM principal directions in equal area upper hemisphere stereoplots. N gives the number of specimens for which results are plotted. For sites where not all AARM measurements were significant, the number of measurements is given in brackets, in addition to the number of specimens with significant AARM.*

Principal AARM directions are shown in Figure 5. Principal remanence directions from specimens of the same site or neighboring sites agree well, in particular for the maximum remanence axis. Like for AMS, the minimum principal axis is generally perpendicular to the trend of the layering.

5 Discussion

5.1 Carriers of remanence and anisotropy

Previous studies report that the mineral responsible for the stable and strong NRM of the rocks in the MCU IVe' layer of the BKS intrusion is hemo-ilmenite [*McEnroe et al.*, 2004a; 2009a; *McEnroe et al.*, 2001b]. Under these circumstances, one would ideally isolate the anisotropy due to hemo-ilmenite and compare the direction and intensity of the NRM to that component of the anisotropy. However, isolating the anisotropy of a high-coercivity low-magnetization mineral that coexists with magnetite is difficult, as has been shown for hematite [*Bilardello and Kodama*, 2009; *Kodama and Dekkers*, 2004]. *Biedermann et al.* [2016] reported that the major component of the AMS for the specimens of the present study is carried by shape and distribution anisotropy of magnetite.

AF demagnetization performed in this study (cf. Figure 3) shows that in most sites ≥ 90% of the NRM is removed below 60 mT, while a small portion of the NRM cannot be removed by AF demagnetization up to 200 mT. This behavior is associated with the presence of two mineralogical remanence carriers, magnetite and hemo-ilmenite, and an additional coercivity distribution of the hemo-ilmenite related to the size of the lamellae. For most sites, removal of the lower-coercivity component drastically decreases the remanence intensity, however, this is not accompanied by major changes in remanence direction, indicating that the remanences carried by both minerals are coaxial, and that the NRM, other than a possible small viscous overprint removed during the first demagnetization step, is, in effect, the characteristic remanence (ChRM). For these sites, it may thus be justified to use the anisotropy carried by magnetite, as described by AMS and AARM, and correlate this to the NRM/ChRM direction and intensity. For consistency, NRM directions of those sites in the north and west that do show directional changes during demagnetization will also be corrected for the anisotropy measured by AMS and AARM. However, these remanence directions and anisotropies may be somewhat biased by the non ChRM-carrying lower coercivity grains, and caution should be exercised when interpreting these results.

5.2 Correlations between NRM directions and magnetic fabrics

NRM inclinations are steeply negative in all sites, however, the declinations change between site locations, synchronously to changes in the orientations of AMS and AARM principal axes. Some inherent variation of NRM directions is expected for a 7 km thick intrusion, due to secular variation of the Earth's magnetic field during the slow cooling. For example, several field reversals have been recorded in the 8 km thick Bushveld Complex [*Cawthorn and Webb*, 2013]. However, the change in NRM declination appears to be systematic when moving along the MCU IVe' layer from the eastern limb of the syncline to the hinge zone in the N, and to the western limb, as does the orientation of the magnetic fabric.

For the majority of specimens, the angle between NRM and maximum susceptibility is less than 50°, and the angle between NRM and minimum susceptibility is more than 45°. The angle between NRM and the maximum AARM is generally less than 30° and thus smaller than the angle between NRM and maximum susceptibility. The NRM is commonly tilted more than 75° away from the minimum AARM axis. A mean paleofield direction of D = 325.9° and I = -80.1° , α_{95} = 4.9° was reported from the Egersund-Ogna anorthosite, which is located to the west of the BKS and acquired its remanent magnetization ~900 Ma ago [*Brown and McEnroe*, 2004]. *Brown and McEnroe* [2015] conducted a paleomagnetic study in the region of the BKS intrusion, and found a mean paleomagnetic direction of D = 303.4° and I = -73.5°, α_{95} = 3.7°. These two directions are at an angle of 8.2°, and based on the test by *McFadden and Lowes* [1981], the two populations may share a common mean at the 95 % confidence interval. Assuming that these describe the direction of the magnetizing field, the NRM observed in this study commonly deviates by an angle of up to 40-50° from the paleofield direction. Figure 6 shows that in most sites and locations, the NRM is tilted away from the paleofield direction and towards the maximum susceptibility and maximum anhysteretic remanence (cf. Figure S1, Supporting Information, for a compilation of data by site).

NRM directions were corrected for anisotropy by multiplying the observed magnetization with the inverse of the (1) susceptibility or (2) remanence susceptibility tensor. AMS-correction was applied to all specimens, as well as site means, and AARM-correction to all specimens on which AARM had been measured. The anisotropy correction changes the NRM directions by up to ca. 20° (both using individual/site mean AMS or AARM), and most directions change by 2 - 12° (AMS) or by 6 - 12° (AARM). For those specimens whose NRM direction did not change significantly during AF demagnetization of the NRM, the AMS-corrected site mean directions are generally closer to the mean paleofield direction, however, some difference between corrected NRM direction and paleofield remains. The anisotropy correction appears to be more successful when using the paleofield as defined by *Brown and McEnroe* [2015], as compared to the paleofield direction from *Brown and McEnroe* [2004], likely because their 2015 paleofield was determined from samples from the BKS. Conversely, for most sites whose AF behavior indicates two components to the NRM with different directions, the angle between the paleofield and NRM direction may increase after the anisotropy correction (Figure 7). In terms of the deviation from the paleofield, not much difference is observed between correcting for AMS or AARM.

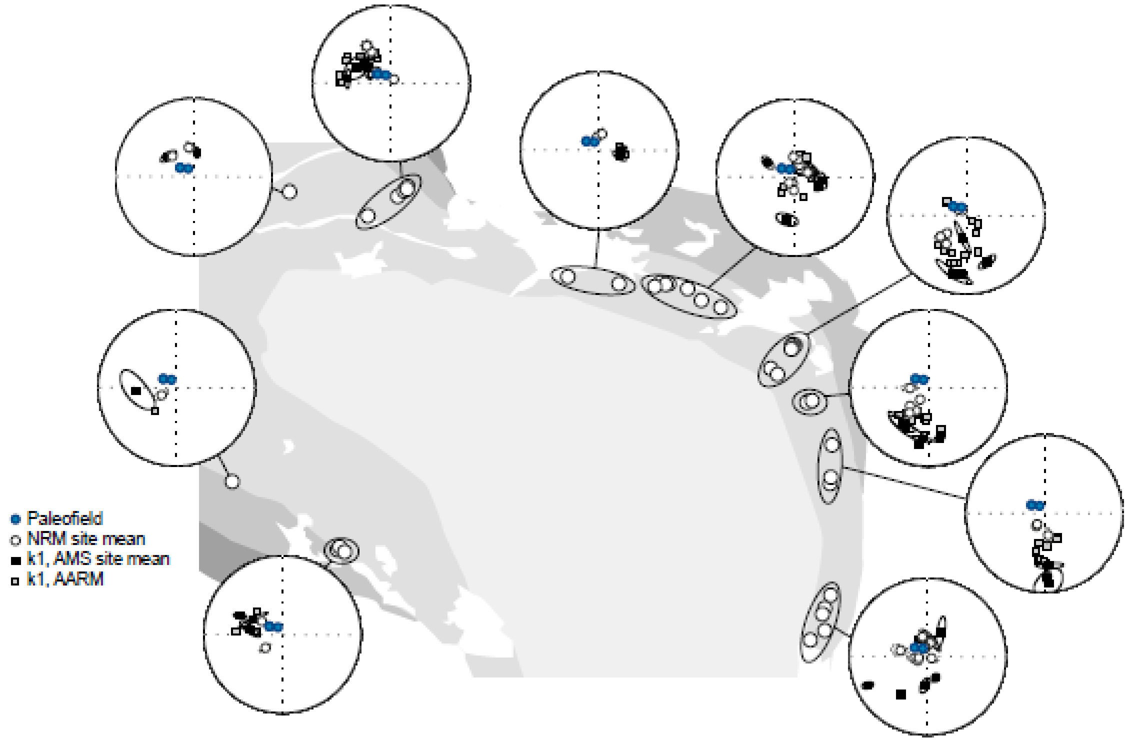

Figure 6*: NRM site means (white circles), maximum susceptibility site means (black squares) and maximum anhysteretic remanences (grey squares) compared to the paleofield directions (blue circles) from Brown and McEnroe (2004; 2015).*

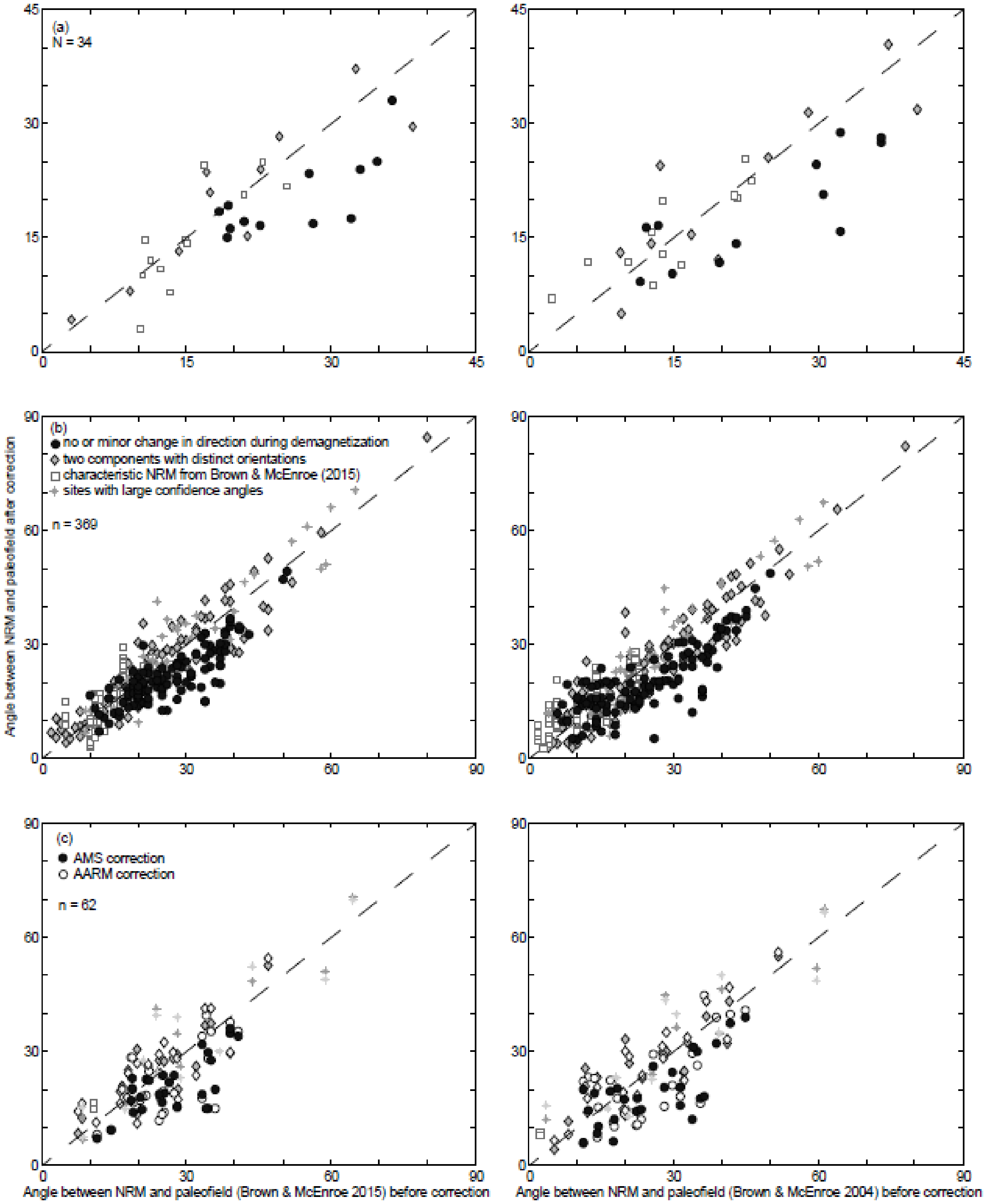

Figure 7*: Angle between NRM and the paleofields as defined by Brown and McEnroe (2004; 2015) before and after anisotropy correction:* ***(a)*** *site means,* ***(b)*** *individual specimens.* ***(c)*** *Comparison between AMS and AARM corrections on the NRM direction for specimens where AARM was measured. Note the different axes for the site mean plots.*

The incomplete restoration of the paleofield direction by the anisotropy corrections indicates that the NRM acquisition process was more anisotropic than the laboratory remanence acquisition, and/or that the NRM resides in (or is stabilized by) a phase that is more anisotropic than the AMS or AARM carrier. The NRM is thought to have been acquired through the formation of hematite-ilmenite interfaces by subsolidus exsolution, and the emergence of a spontaneous magnetization in the interfacial layers (lamellar magnetism), which is thus a chemical remanence [*Robinson et al.*, 2004]. The orientation of this magnetization is crystallographically constrained, so the remanence acquisition is extremely anisotropic on the grain scale [*Robinson et al.*, 2006]. The high intensity of the NRM, combined with the high concentration of magnetite in these specimens, suggests that magnetite probably contributes significantly to the NRM, perhaps involving interaction of the hemo-ilmenite lamellar magnetism with the magnetite magnetism. Magnetite by itself may not have remained stably magnetized in the direction of the Proterozoic magnetic field, but changed its magnetization direction over time, to adjust to the present field. However, in the presence of hemo-ilmenite, which, due to its remanence generates a secondary field, the magnetite stayed magnetized in a direction similar to the remanence of the hemo-ilmenite. It appears that this effect is strongest in the eastern part of the intrusion, where the NRM is most intense, and the NRM directions do not change, or show only minor changes, during AF demagnetization. Even though a large part of the remanence is removed in small (< 100 mT) laboratory fields, indicating a dominant magnetite contribution, its direction may thus be controlled by the crystallographic preferred orientation, and associated magnetic anisotropy, of hemo-ilmenite. This process would explain why the NRM direction cannot be completely restored by correcting for the effect of magnetite-dominated AMS or AARM.

The present study illustrates the importance of correcting NRM deflections with the magnetic fabric of the mineral that carries the remanence, which may be different from the mineral that dominates the AMS. In addition, it shows that interactions between different minerals can add to the complexity of such studies.

5.3 NRM intensity and anisotropy

NRM intensity varies from <1 A/m to 60 A/m and is strongest for specimens from sites close to Heskestad (i.e. sites BK112, BK113, BK114). One aim of this study was to investigate whether and how the intensity of the NRM is affected by anisotropy. The magnetization of an anisotropic rock is strongest when it is magnetized parallel to its easy axis. Thus, in a simple one-phase system, the remanence is expected to be strongest in specimens where the angle between the paleofield direction and the maximum principal axis of the AARM or AMS is smallest. Similarly, one would expect the NRM intensity to increase with increasing angle between the minimum AARM or AMS principal axis and the direction of the magnetizing field, and reach a maximum when they are perpendicular to each other. Additionally, the NRM intensity is expected to be strongest when it is parallel to the maximum susceptibility or remanence, and perpendicular to the minimum susceptibility and remanence.

In the BKS intrusion, the angle between the paleofield direction and the maximum principal axis of the AMS or AARM ellipsoid varies from ca. 5° to 90° and from 5° to 60°, respectively. The angle between the minimum principal axis and the field ranges from 20° (AMS) or 50° (AARM) to 90°. The NRM is deflected up to ca. 50° from the paleofield, and makes an angle typically up to around 50° and 30° with the maximum susceptibility and anhysteretic remanence, respectively (Figure 8). Hence, a large range of directional relationships between the paleofield and magnetic fabric is covered.

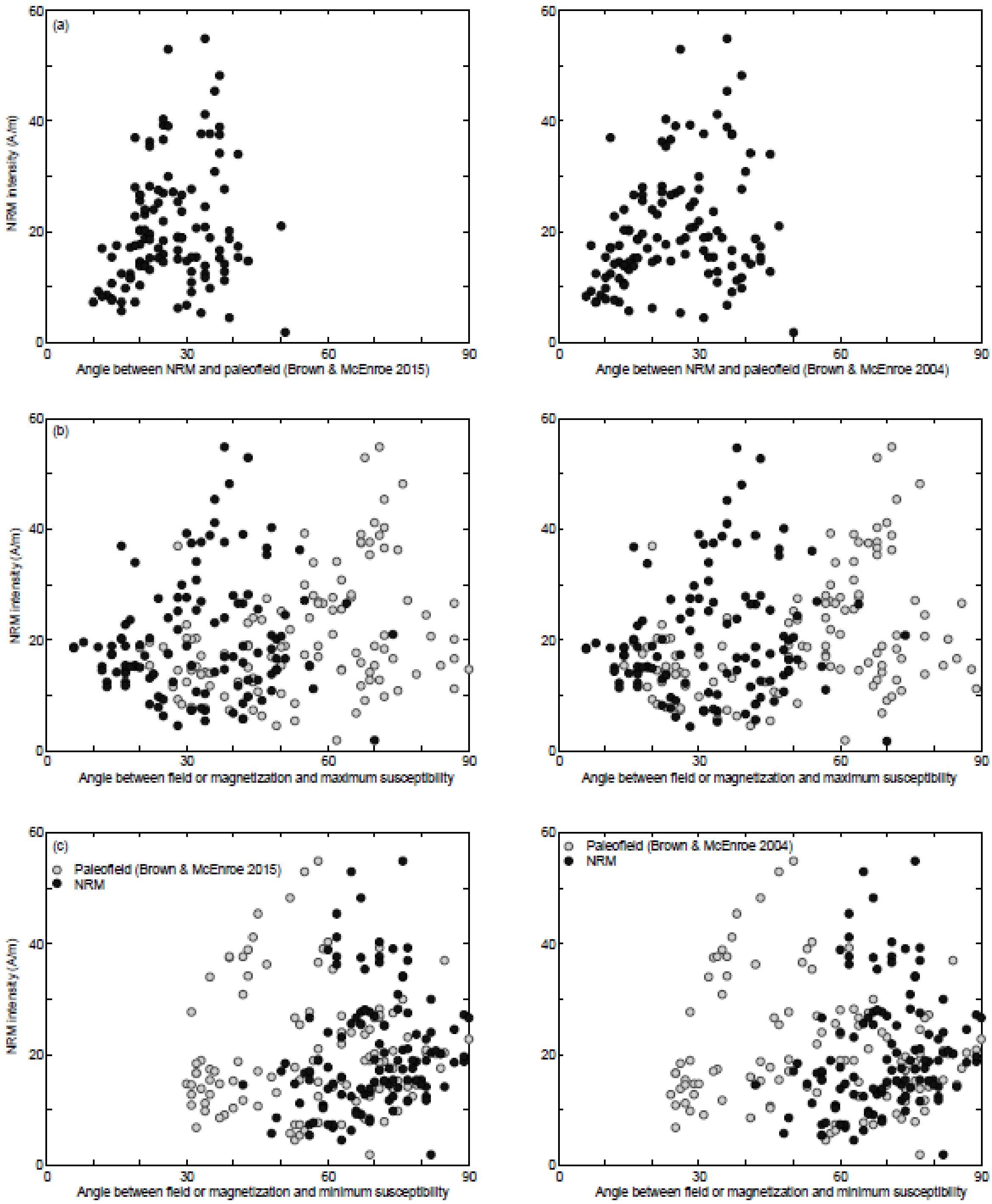

***Figure 8**: NRM intensity as a function of the relative orientation of magnetic fabric, paleofield, and NRM; **(a)** angle between NRM and paleofield, **(b)** angle between maximum susceptibility axis and paleofield (grey) or NRM (black), **(c)** angle between minimum susceptibility axis and paleofield (grey) or NRM (black).*

Only samples with no or minor changes in the magnetization direction during AF demagnetization will be considered to investigate the possible dependence of NRM intensity on the relative orientation of paleofield, magnetic fabric and magnetization. In samples whose NRM consists of several components with different orientations, both intensity and direction of NRM are affected by secondary components or viscous magnetization.

No clear correlation is observed between the NRM intensity and the orientation of the paleofield or NRM with respect to the magnetic fabric. To account for different concentrations of magnetic minerals in each specimen, the NRM intensity was normalized by the mean susceptibility, and the mean anhysteretic remanence, yet still no clear correlations are observed between the NRM intensity and directional relationships. This may indicate that other factors, such as the degree and shape of the anisotropy ellipsoid, or the properties of the magnetic minerals, e.g. chemical composition, grain size, or exsolution textures, which may vary along the layer, play a larger role in influencing the NRM intensity than the orientation of the magnetic fabric does. Another possible explanation is that both mean susceptibility and AARM provide estimates of the magnetite content, whereas the NRM intensity is also influenced by the abundance of lamellae interfaces in the hemo-ilmenite. No simple estimate for the latter can be obtained based on magnetic data alone. This is further illustrated by specimens from site BK2016_26. In this site, all specimens have similar density, mean susceptibility and AMS, however, the intensity of the NRM is bimodal, with ca. an order of magnitude difference for the two modes. Thus, whereas magnetic anisotropy of magnetite clearly causes NRM deflection in the BKS layered intrusion, it appears not to have a major influence on the strength of the remanence.

6 Conclusions

The rocks from the MCU IVe' layer of the BKS layered intrusion carry a strong NRM, which is steeply negative. The NRM declination appears to change systematically when moving along the layer from E to N to W, at the same time as the orientation of the magnetic fabric changes. Previous studies have shown that the NRM is carried by hemo-ilmenite, and the magnetic anisotropy is dominated by magnetite. Preferred orientation of minerals is observed in all specimens, and magnetic fabrics are strong, with P up to 2.7 for low-field AMS, and up to 3.6 for AARM. The minimum susceptibility or anhysteretic remanence are approximately normal to the macroscopic layering or foliation.

The NRM appears to be deflected away from the paleofield directions as defined by *Brown and McEnroe* [2004], or *Brown and McEnroe* [2015], and towards the maximum susceptibility or anhysteretic remanence. Correcting NRM directions for magnetic fabrics leads to smaller deviations from the paleofield direction in specimens whose NRM directions remain the same during AF demagnetization, but the corrected magnetizations do not coincide with the paleofield direction, likely because the NRM is carried by both hemo-ilmenite and magnetite, but the AMS is dominated by magnetite. In specimens whose NRM contains components with different orientations, correcting for anisotropy can lead to a larger deflection. This is due to the effects of a later overprint with a differently oriented magnetization. No clear correlation has been found between the NRM intensity and orientation of the magnetic fabric with respect to the paleofield direction. More work is needed to investigate the influence of magnetic anisotropy on the intensity of the NRM and on magnetic anomalies.

Acknowledgments and Data

Alexander Michels, NTNU, is thanked for help during fieldwork. Bjarne S.G. Almqvist, Uppsala University, kindly provided access to their MFK1 susceptibility bridge for initial AMS measurements, and Morgan Ganerød, Norwegian Geological Survey (NGU), is thanked for access to their JR6 spinner magnetometer. We are grateful to Peat Solheid for assistance during sample preparation and measurements at the Institute for Rock Magnetism (IRM), University of Minnesota. This study was funded by the Swiss National Science Foundation (project P2EZP2-155517 to A. Biedermann), NTNU, Research Council of Norway (grant 222666 to S. McEnroe), and a visiting fellowship at the IRM, which is supported by the Instruments and Facilities program of the US National Science Foundation, Division of Earth Sciences. Fátima Martín-Hernández and Martin Chadima are acknowledged for their constructive reviews which helped to improve the manuscript and Michael Walter for editorial handling of the manuscript. Additional data tables and figures are available in the Supporting Information.

References

Aitken, M. J., P. A. Alcock, G. D. Bussell, and C. J. Shaw (1981), Archaeomagnetic determineation of the past geomagnetic intensity using ancient ceramics: allowance for anisotropy, *Archaeomatry*, *23*(1), 53-64.

Anson, G. L., and K. P. Kodama (1987), Compaction-induced inclination shallowing of the post-depositional remanent magnetization in a synthetic sediment, *Geophysical Journal of the Royal Astronomical Society*, *88*(3), 673-692.

Biedermann, A. R., F. Heidelbach, M. Jackson, D. Bilardello, and S. A. McEnroe (2016), Magnetic fabrics in the Bjerkreim Sokndal Layered Intrusion, Rogaland, Southern Norway, *Tectonophysics*, *in review*.

Bilardello, D., and K. P. Kodama (2009), Measuring remanence anisotropy of hematite in red beds: anisotropy of high-field isothermal remanence magnetization (hf-AIR), *Geophysical Journal International*, *178*(3), 1260-1272, doi:10.111/j.1365-246X.2009.04231.x.

Bilardello, D., and K. P. Kodama (2010a), A new inclination shallowing correction of the Mauch Chunk Formation of Pennsylvania, based on high-field AIR results: Implications for the Carboniferous North American APW path and Pangea reconstructions, *Earth and Planetary Science Letters*, *299*(1-2), 218-227, doi:10.1016/j.epsl.2010.09.002.

Bilardello, D., and K. P. Kodama (2010b), Rock magnetic evidence for inclination shallowing in the early Carboniferous Deer Lake Group red beds of western Newfoundland, *Geophysical Journal International*, *181*(1), 275-289, doi:10.1111/j.1365-246X.2010.04537.x.

Bolle, O., H. Diot, and J.-C. Duchesne (2000), Magnetic fabric and deformation in charnockitic igneous rocks of the Bjerkreim-Sokndal layered intrusion (Rogaland, Southwest Norway), *Journal of Structural Geology*, *22*, 647-667.

Bolle, O., R. I. F. Trindade, J. L. Bouchez, and J. C. Duchesne (2002), Imaging downward granitic magma transport in the Rogaland Igneous Complex, SW Norway, *Terra Nova*, *14*, 87-92.

Bressler, S. C., and D. P. Elston (1980), Declination and inclination errors in experimentally deposited specularite-bearing sand, *Earth and Planetary Science Letters*, *48*, 227-232.

Brown, L. L., and S. A. McEnroe (2004), Palaeomagnetism of the Egersund-Ogna anorthosite, Rogaland, Norway, and the position of Fennoscandia in the Late Proterozoic, *Geophysical Journal International*, *158*(2), 479-488, doi:10.1111/j.1365-246X.2004.02349.x.

Brown, L. L., and S. A. McEnroe (2012), Paleomagnetism and magnetic mineralogy of Grenville metamorphic and igneous rocks, Adirondack Highlands, USA, *Precambrian Research*, *212-213*, 57-74, doi:10.1016/j.precamres.2012.04.012.

Brown, L. L., and S. A. McEnroe (2015), 916 Ma Pole for southwestern Baltica: palaeomagnetism of the Bjerkreim-Sokndal layered intrusion, Rogaland Igneous

Complex, southern Norway, *Geophysical Journal International*, *203*(1), 567-587, doi:10.1093/gji/ggv299.

Cawthorn, R. G., and S. J. Webb (2013), Cooling of the Bushveld Complex, South Africa: Implications for paleomagnetic reversals, *Geology*, *41*(6), 687-690.

Cogné, J. P., and H. Perroud (1988), Anisotropy of magnetic susceptibility as a strain gauge in the Flamanville granite, NW France, *Physics of the Earth and Planetary Interiors*, *51*, 264-270.

Duchesne, J. C. (1972), Iron-Titanium Oxide Minerals in the Bjerkreim-Sogndal Massif, South-western Norway, *Journal of Petrology*, *13*, 57-81.

Duchesne, J. C. (1999), Fe-Ti deposits in Rogaland anorthosites (South Norway): geochemical characteristics and problems of interpretation, *Mineralium Deposita*, *34*, 182-198.

Duchesne, J. C. (2001), The Rogaland Intrusive Massifs - an excursion guide, *NGU Report*, *2001.029*, 139 pp.

Feinberg, J. M., H.-R. Wenk, G. R. Scott, and P. R. Renne (2006), Preferred orientation and anisotropy of seismic and magnetic properties in gabbronorites from the Bushveld layered intrusion, *Tectonophysics*, *420*(3-4), 345-356, doi:10.1016/j.tecto.2006.03.017.

Ferré, E. C., C. Bordarier, and J. S. Marsh (2002), Magma flow inferred from AMS fabrics in a layered mafic sill, Insizwa, South Africa, *Tectonophysics*, *354*, 1-23.

Ferré, E. C., J. Wilson, and G. Gleizes (1999), Magnetic susceptibility and AMS of the Bushveld alkaline granites, South Africa, *Tectonophysics*, *307*, 113-133.

Fuller, M. D. (1960), Anisotropy of susceptibility and the natural remanent magnetization of some Welsh slates, *Nature*, *186*, 790-792.

Fuller, M. D. (1963), Magnetic anisotropy and paleomagnetism, *Journal of Geophysical Research*, *68*(1), 293-309.

Girdler, R. W. (1961), Some preliminary measurements of anisotropy of magnetic susceptibility of rocks, *Geophysical Journal of the Royal Astronomical Society*, *5*(3), 197-206.

Halls, H. C., and J. A. Hanes (1999), Paleomagnetism, anisotropy of magnetic susceptibility, and argon-argon geochronology of the Clearwater anorthosite, Saskatchewan, Canada, *Tectonophysics*, *312*(2-4), 235-248.

Hargraves, R. B. (1959), Magnetic anisotropy and remanent magnetism in hemo-ilmenite from ore deposits at Allard Lake, Quebec, *Journal of Geophysical Research*, *64*(10), 1565-1578, doi:10.1029/JZ064i010p01565.

Huang, W., D. J. J. van Hinsbergen, M. Maffione, D. A. Orme, G. Dupont-Nivet, C. Guilmette, L. Ding, Z. Guo, and P. Kapp (2015), Lower Cretaceous Xigaze ophiolites formed in the Gangdese forearc: Evidence from paleomagnetism, sediment provenance, and stratigraphy, *Earth and Planetary Science Letters*, *415*, 142-153, doi:10.1016/j.epsl.2015.01.032.

Jackson, M. J., S. K. Banerjee, J. A. Marvin, R. Lu, and W. Gruber (1991), Detrital remanence, inclination errors, and anhysteretic remanence anisotropy: quantitative model and experimental results, *Geophysical Journal International*, *104*, 95-103.

Jelinek, V. (1977), The statistical theory of measuring anisotropy of magnetic susceptibility of rocks and its application.

Jelinek, V. (1981), Characterization of the magnetic fabric of rocks, *Tectonophysics*, *79*, T63-T67.

Jelinek, V. (1984), On a mixed quadratic invariant of the magnetic susceptibility tensor, *Journal of Geophysics - Zeitschrift Fur Geophysik*, *56*(1), 58-60.

Jelinek, V. (1996), Measuring anisotropy of magnetic susceptibility on a slowly spinning specimen - basic theory, *AGICO Print No. 10*.

Karlsen, T. A., H. Schiellerup, S. A. McEnroe, L. P. Nilsson, and A. Korneliussen (1996), Current research on ilmenite in the Egersund Province, *NGU Report*, *96.059*, 38 pp.
King, R. F. (1955), The remanent magnetism of artificially deposited sediments, *Geophysical Supplements to the Monthly Notices of the Royal Astronomical Society*, *7*(3), 115-134, doi:10.1111/j.1365-246X.1955.tb06558.x.
Kirker, A. I., and E. McClelland (1997), Deflection of magnetic remancence during progressive cleavage development in the Pembrokeshsire Old Red Sandstone, *Geophysical Journal International*, *130*, 240-250.
Kligfield, R., W. Lowrie, A. Hirt, and A. W. B. Siddans (1983), Effect of progressive deformation on remanent magnetization of Permian redbeds from the Alpes Maritimes (France), *Tectonophysics*, *97*, 59-85.
Kodama, K. P., and M. J. Dekkers (2004), Magnetic anisotropy as an aid to identifying CRM and DRM in red sedimenetary rocks, *Studia Geophysica Et Geodaetica*, *48*, 747-766.
Korneliussen, A., S. A. McEnroe, L. P. Nilsson, H. Schiellerup, H. Gautneb, G. B. Meyer, and L. R. Størseth (2000), An overview of titanium deposits in Norway, *NGU Bulletin*, *436*, 27-38.
Krijgsman, W., and L. Tauxe (2004), Shallow bias in Mediterranean paleomagnetic directions caused by inclination error, *Earth and Planetary Science Letters*, *222*(2), 685-695, doi:10.1016/j.epsl.2004.03.007.
Lovlie, R., and T. Torsvik (1984), Magnetic remanence and fabric properties of laboratory deposited hematite-bearing red sandstone, *Geophysical Research Letters*, *11*, 229-232.
Lowrie, W., A. M. Hirt, and R. Kligfield (1986), Effects of tectonic deformation on the remanent magnetization of rocks, *Tectonics*, *5*(5), 713-722.
Maes, S. M., B. Tikoff, E. C. Ferré, P. E. Brown, and J. D. Miller Jr. (2007), The Sonju Lake layered intrusion, northeast Minnesota: Internal structure and emplacement history inferred from magnetic fabrics, *Precambrian Research*, *157*(1-4), 269-288, doi:10.1016/j.precamres.2007.02.021.
Maquil, R., and J. C. Duchesne (1984), Géothermométrie par les pyroxènes et mise en place du massif anorthositique d'Egersund-Ogna (Rogaland, Norvège Mèridionale), *Annales de la Société Géologique de Belgique*, *T. 107*, 27-49.
McEnroe, S. A., and L. L. Brown (2000), A closer look at remanence-dominated aeromagnetic anomalies: Rock magnetic properties and magnetic mineralogy of the Russell Belt microcline-sillimanite gneiss, northwest Adirondack Mountains, New York, *Journal of Geophysical Research*, *105*(B7), 16437-16456, doi:10.1029/2000jb900051.
McEnroe, S. A., L. L. Brown, and P. Robinson (2004a), Earth analog for Martian magnetic anomalies: remanence properties of hemo-ilmenite norites in the Bjerkreim-Sokndal intrusion, Rogaland, Norway, *Journal of Applied Geophysics*, *56*(3), 195-212, doi:10.1016/j.jappgeo.2004.07.002.
McEnroe, S. A., L. L. Brown, and P. Robinson (2009a), Remanent and induced magnetic anomalies over a layered intrusion: Effects from crystal fractionation and magma recharge, *Tectonophysics*, *478*(1-2), 119-134, doi:10.1016/j.tecto.2008.11.021.
McEnroe, S. A., B. Carter-Stiglitz, R. J. Harrison, P. Robinson, K. Fabian, and C. McCammon (2007a), Magnetic exchange bias of more than 1 Tesla in a natural mineral intergrowth, *Nature Nanotechnology*, *2*, 631-634.
McEnroe, S. A., M. D. Dyar, and L. B. Brown (2002), Magnetic signatures on planets without magnetic fields, *Lunar and Planetary Science*, *XXXIII*, 1287-1288.
McEnroe, S. A., K. Fabian, P. Robinson, C. Gaina, and L. L. Brown (2009b), Crustal Magnetism, Lamellar Magnetism and Rocks That Remember, *Elements*, *5*(4), 241-246, doi:10.2113/gselements.5.4.241.

McEnroe, S. A., R. J. Harrison, P. Robinson, U. Golla, and M. J. Jercinovic (2001a), Effect of fine-scale microstructures in titanohematite on the acquisition and stability of natural remanent magnetization in granulite facies metamorphic rocks, southwest Sweden: Implications for crustal magnetism, *Journal of Geophysical Research*, *106*(B12), 30523, doi:10.1029/2001jb000180.

McEnroe, S. A., P. Robinson, F. Langenhorst, C. Frandsen, M. P. Terry, and T. B. Ballaran (2007b), Magnetization of exsolution intergrowths of hematite and ilmenite: Mineral chemistry, phase relations, and magnetic properties of hemo-ilmenite ores with micron- to nanometer-scale lamellae from Allard Lake, Quebec, *Journal of Geophysical Research*, *112*(B10), doi:10.1029/2007jb004973.

McEnroe, S. A., P. Robinson, N. Miyajima, K. Fabian, D. Dyar, and E. Sklute (2016), Lamellar magnetism and exchange bias in billion-year-old titanohematite with nanoscale ilmenite exsolution lamellae: 1. Mineral and Magnetic characterization, *Geophysical Journal International*, *206*, 470-486.

McEnroe, S. A., P. Robinson, and P. Panish (1996), Rock-magnetic properties, oxide mineralogy, and mineral chemistry in relation to aeromagnetic interpretation and the search for ilmenite reserves, *NGU Report*, *96.060*.

McEnroe, S. A., P. Robinson, and P. T. Panish (2001b), Aeromagnetic anomalies, magnetic petrology, and rock magnetism of hemo-ilmenite- and magnetite-rich cumulate rocks from the Sokndal Region, South Rogaland, Norway, *American Mineralogist*, *86*, 1447-1468.

McEnroe, S. A., J. R. Skilbrei, P. Robinson, F. Heidelbach, F. Langenhorst, and L. L. Brown (2004b), Magnetic anomalies, layered intrusions and Mars, *Geophysical Research Letters*, *31*(19), doi:10.1029/2004gl020640.

McFadden, P. L., and F. J. Lowes (1981), The discrimination of mean directions drawn from Fisher distributions, *Geophysical Journal of the Royal Astronomical Society*, *67*(1), 19-33.

Michot, P. (1960), La géologie de la catazone: le problème des anorthosites, la palingenèse basique et la tectonique catazonale dans le Rogaland méridional (Norvège méridionale), *NGU Bulletin*, *212*, 1-54.

Michot, P. (1965), Le magma plagioclasique, *Geologische Rundschau*, *54*(2), 956-976.

Muttoni, G., D. V. Kent, E. Garzanti, P. Brack, N. Abrahamsen, and M. Gaetani (2003), Early Permian Pangea 'B' to Late Permian Pangea 'A', *Earth and Planetary Science Letters*, *215*, 379-394, doi:10.1016/S0012-821X(03)00452-7.

Nabi, H. S., and R. Pentcheva (2010), Origin of Interface Magnetism in Fe2O3/FeTiO3 Heterostructures, in *High Performance Computing in Science and Engineering*, edited by S. Wagner, et al., Springer, Berlin, Germany, doi:10.1007/978-3-642-13872-0.

O'Driscoll, B., R. B. Hargraves, C. H. Erneleus, V. Troll, C. H. Donaldson, and R. J. Reavy (2007), Magmatic lineations inferred from anisotropy of magnetic susceptibility fabrics in units 8, 9, and 10 of the Rum Eastern Layered Series, NW Scotland, *Lithos*, *98*(1-4), 27-44, doi:10.1016/j.lithos.2007.01.009.

O'Driscoll, B., E.C. Ferre, C.T.E. Stevenson, and C. Magee (2015), The Significance of Magnetic Fabric in Layered Mafic-Ultramafic Intrusions, in *Layered Intrusions*, edited by B. Charlier et al., Springer, Dordrecht, Germany.

Paludan, J., U. B. Hansen, and N. Ø. Olesen (1994), Structural evolution of the Precambrian Bjerkreim-Sokndal intrusion, South Norway, *Norsk Geologisk Tidsskrift*, *74*, 185-198.

Pentcheva, R., and H. S. Nabi (2008), Interface magnetism in Fe_2O_3/$FeTiO_3$ heterostructures, *Physical Review B*, *77*(17), doi:10.1103/PhysRevB.77.172405.

Robins, B., and J. R. Wilson (2001), The Bjerkreim-Sokndal layered intrusion, in *The Rogaland Intrusive Massifs - an excursion guide*, edited by J. C. Duchesne, NGU Report, Trondheim, Norway.

Robinson, P., K. Fabian, S. A. McEnroe, and F. Heidelbach (2013), Influence of lattice-preferred orientation with respect to magnetizing field on intensity of remanent magnetization in polycrystalline hemo-ilmenite, *Geophysical Journal International*, *192*(2), 514-536, doi:10.1093/gji/ggs046.

Robinson, P., R. J. Harrison, S. A. McEnroe, and R. B. Hargraves (2002), Lamellar magnetism in the haematite-ilmenite series as an explanation for strong remanent magnetization, *Nature*, *418*(6897), 517-520, doi:10.1038/nature00924.

Robinson, P., R. J. Harrison, S. A. McEnroe, and R. B. Hargraves (2004), Nature and origin of lamellar magnetism in the hematite-ilmenite series, *American Mineralogist*, *89*, 725-747.

Robinson, P., F. Heidelbach, A. M. Hirt, S. A. McEnroe, and L. L. Brown (2006), Crystallographic-magnetic correlations in single-crystal haemo-ilmenite: new evidence for lamellar magnetism, *Geophysical Journal International*, *165*(1), 17-31, doi:10.1111/j.1365-246X.2006.02849.x.

Robinson, P., P. T. Panish, and S. A. McEnroe (2001), Minor element chemistry of hemo-ilmenite and magnetite in cumulate rocks from the Sokndal Region, South Rogaland, Norway, *American Mineralogist*, *86*, 1469-1476.

Rogers, J., J. M. W. Fox, and M. J. Aitken (1979), Magnetic anisotropy in ancient pottery, *Nature*, *277*, 644-646, doi:10.1038/277644a0.

Schärer, U., E. Wilmart, and J. C. Duchesne (1996), The short duration and anorogenic character of anorthosite magmatism: U-Pb dating of the Rogaland complex, Norway, *Earth and Planetary Science Letters*, *139*, 335-350.

Selkin, P. A., J. S. Gee, L. Tauxe, W. P. Meurer, and A. J. Newell (2000), The effect of remanence anisotropy on paleointensity estimates: a case study from the Archean Stillwater Complex, *Earth and Planetary Science Letters*, *183*, 403-416.

Stephenson, A., S. Sadikun, and D. K. Potter (1986), A theoretical and experimental comparison of the anisotropies of magnetic susceptibility and remanence in rocks and minerals, *Geophysical Journal of the Royal Astronomical Society*, *84*, 185-200.

Tan, X., and K. Kodama (1998), Compaction-corrected inclinations from southern California Cretaceous marine sedimentary rocks indicate no paleolatitudinal offset for the Peninsular Ranges terrane, *Journal of Geophysical Research - Solid Earth*, *103*(B11), 27169-27192.

Tan, X., and K. Kodama (2002), Magnetic anisotropy and paleomagnetic inclination shallowing in red beds: evidence from the Mississippian Mauch Chunk Formation, Pennsylvania, *Journal of Geophysical Research - Solid Earth*, *107*(B11), EPM9-1 - EPM9-17, doi:10.1029/2001JB001636.

Tarduno, J. A. (1990), Absolute inclination values from deep sea sediments: a reexamination of the Cretaceous Pacific record, *Geophysical Research Letters*, *17*, 101-104.

Tauxe, L., and D. V. Kent (1984), Properties of a detrital remanence carried by hematite from study of modern river deposits and laboratory redeposition experiments, *Geophysical Journal of the Royal Astronomical Society*, *77*, 543-561.

Tauxe, L., and D. V. Kent (2004), A simplified statistical model for the geomagnetic field and the detection of shallow bias in paleomagnetic inclinations: was the ancient magnetic field dipolar?, in *Timescales of the Paleomagnetic Field*, edited by J. E. T. Channell, D. V. Kent, W. Lowrie and J. Meert, AGU, Washington DC, USA.

Tauxe, L., K. P. Kodama, and D. V. Kent (2008), Testing corrections for paleomagnetic inclination error in sedimentary rocks: A comparative approach, *Physics of the Earth and Planetary Interiors*, *169*(1-4), 152-165, doi:10.1016/j.pepi.2008.05.006.

Uyeda, S., M. D. Fuller, C. Belshe, and R. W. Girdler (1963), Anisotropy of magnetic susceptibility of rocks and minerals, *Journal of Geophysical Research*, *68*(1), 279-291.

Vaughn, J., K. P. Kodama, and D. P. Smith (2005), Correction of inclination shallowing and its tectonic implications: The Cretaceous Perforada Formation, Baja California, *Earth and Planetary Science Letters*, *232*(1-2), 71-82, doi:10.1016/j.epsl.2004.11.026.

Wilson, J. R., B. Robins, F. M. Nielsen, J. C. Duchesne, and J. Vander Auwera (1996), The Bjerkreim-Sokndal layered intrusion, Southwest Norway, in *Layered Intrusions*, edited by R. G. Cawthorn, pp. 231-255, Elsevier, Amsterdam.

Table 1: Sample list with MCU layer, site mean NRM, and site mean AMS data. * indicates samples whose NRM data were taken from Brown and McEnroe 2015.

		NRM							AMS																		AMS-corrected NRM	
Site	Unit	Number o	Intensity (A/m)	D	I	κ	α95		Number o	mean (SI)	k1	D1	I1	onfidence ellipse, k1		k2	D2	I2	onfidence ellipse, k2		k3	D3	I3	onfidence ellipse, k3			D	I
BK2015_2	MCU IVe'	8	43.0	209.7	-63.2	160.4	4.4		8	1.75E-01	1.402	9.7	27.7	4.2	2.2	0.892	116.5	28.9	6.7	2.2	0.706	244.3	47.9	6.7	4.1		226.4	-79.3
BK2015_3	MCU IVe'	10	22.6	226.2	-63.4	90.8	5.1		10	1.02E-01	1.176	36.3	41.5	13.9	4.4	0.984	154.1	27.8	12.0	8.4	0.840	266.5	35.9	12.9	7.1		225.7	-69.2
BK2015_4	MCU IVe'	8	33.4	218.2	-57.5	53.8	7.6		8	1.34E-01	1.247	7.5	34.8	9.8	2.7	0.953	106.2	12.3	9.8	7.5	0.800	212.6	52.5	7.7	3.1		232.3	-64.9
BK2015_5	MCU IVe'	6	25.7	217.2	-75.7	221.6	4.5		6	1.46E-01	1.254	29.6	41.3	22.5	5.7	0.930	141.3	22.9	22.1	6.8	0.816	252.0	40.0	12.7	6.6		208.4	-86.8
BK2015_6	MCU IVe'	6	15.5	227.8	-62.4	338.0	6.6		6	1.26E-01	1.267	3.8	27.5	4.0	2.1	0.924	100.3	12.2	5.2	2.2	0.809	211.8	59.5	4.1	2.0		250.7	-69.1
BK2015_7	MCU IVe'	15	13.3	231.3	-55.4	25.6	7.4		15	1.12E-01	1.214	13.3	26.3	20.1	4.3	0.964	110.6	14.6	20.6	7.9	0.822	226.7	59.4	10.0	5.8		243.3	-62.2
BK2015_8	MCU IVe'	2	14.9	202.0	-57.7	30.9	16.8		4	1.18E-01	not enough for statistics																NaN	NaN
BK2015_9	MCU IVe'	17	17.7	215.5	-54.0	82.6	3.9		17	1.04E-01	1.217	6.0	25.5	8.3	2.0	0.946	103.4	15.2	14.2	5.9	0.837	221.1	59.7	13.2	2.2		226.0	-61.3
BK2015_10	MCU IVe'	5	14.2	212.5	-70.7	6.6	32.3		5	8.22E-02	1.087	338.1	39.7	41.9	8.9	0.985	244.0	4.8	42.6	17.0	0.927	148.3	49.9	43.9	15.2		225.6	-72.4
BK2015_11	MCU IVe'	5	11.9	102.8	-76.3	41.9	12.0		5	7.86E-02	1.162	335.9	36.3	9.8	4.1	1.005	83.1	21.9	7.5	5.6	0.833	197.4	45.5	8.5	4.1		63.8	-75.8
BK2015_13	MCU IVe'	16	16.2	22.6	-76.4	82.3	4.1		16	8.97E-02	1.249	254.8	69.7	11.0	4.8	0.898	77.8	20.3	38.7	4.7	0.853	347.4	1.0	39.1	5.2		359.4	-74.4
BK2015_14	MCU IVe'	13	18.1	10.5	-71.4	569.2	1.7		13	8.81E-02	1.278	250.8	73.6	5.3	3.5	0.885	82.5	16.1	22.2	3.1	0.838	351.6	3.1	22.2	4.8		355.8	-65.6
BK2015_15	MCU IVe'	9	16.3	353.6	-83.0	14.6	13.9		9	9.71E-02	1.214	11.4	67.1	18.7	2.5	0.917	104.0	1.1	35.4	8.4	0.869	194.5	22.9	36.0	8.6		2.3	-74.4
BK2015_16	MCU IVe'	7	13.2	195.0	-83.6	95.1	6.2		7	8.40E-02	1.105	9.8	44.5	10.9	6.2	0.973	269.4	10.4	15.9	9.3	0.922	169.3	43.6	15.5	6.9		229.8	-88.2
BK2015_17	MCU IVe'	7	23.6	356.4	-68.8	100.6	6.0		7	1.51E-01	1.325	277.4	61.1	8.5	4.6	0.928	93.0	28.8	7.2	4.0	0.747	184.1	1.9	8.7	5.3		344.7	-56.4
BK2015_17_ChRM				42.9	-74.6																							
BK2015_18	MCU IVe'	8	33.4	213.0	-74.3	320.4	3.1		8	9.25E-02	1.178	354.2	34.2	13.0	3.3	0.987	111.5	34.0	16.4	3.4	0.835	232.7	37.5	14.2	4.6		229.1	-81.0
BK2015_20	MCU IVe'	7	29.2	213.4	-76.4	208.6	4.2		7	1.14E-01	1.248	357.7	20.0	6.6	3.4	0.931	115.5	52.0	5.9	5.2	0.821	255.2	30.8	6.6	3.8		236.2	-83.1
BK2015_21	MCU IVe'	8	20.3	170.1	-67.0	41.0	8.8		8	6.51E-02	1.138	356.1	13.6	18.7	10.5	1.000	206.3	74.4	19.0	4.7	0.862	87.9	7.6	11.4	6.5		170.7	-70.5
BK2015_22	MCU IVe	6	3.4	345.3	-68.4	74.1	7.8		6	1.34E-01	1.286	195.7	71.9	14.5	3.0	0.911	300.8	4.9	24.3	7.2	0.802	32.3	17.4	22.2	2.7		335.7	-66.1
BK2015_23	MCU IVe	21	5.7	327.0	-42.8	20.5	7.2		21	1.07E-01	1.182	113.7	50.4	13.8	10.1	0.994	315.4	37.6	11.0	7.1	0.824	217.0	10.8	13.4	7.8		337.1	-40.0
BK2015_24	MCU IVc	11	2.3	310.5	-71.2	216.8	3.1		11	1.32E-02	1.212	121.9	55.5	5.2	4.7	0.923	304.6	34.5	21.0	4.2	0.864	213.7	1.2	20.9	4.7		317.3	-75.5
BK2015_24_ChRM				43.4	-78.7																							
BK2015_26	MCU IVb	8	42.3 and 4.5	189.6	-56.9	16.2	12.3		8	2.76E-02	1.175	96.9	44.2	9.5	2.8	0.992	308.1	41.3	8.5	2.6	0.833	203.3	16.2	11.3	1.0		167.0	-40.3
BK2015_27	MCU IVd	10	0.9	36.4	-84.8	808.7	1.7		10	2.99E-03	1.107	129.8	56.0	2.7	1.2	0.977	307.0	34.0	6.7	2.5	0.917	37.9	1.3	6.7	1.6		67.0	-83.3
BK2015_27_ChRM				347.0	-80.8																							
BK2015_28	MCU IVe	9	4.3	328.5	-51.2	73.3	6.1		9	9.70E-02	1.130	123.1	60.8	12.0	5.1	1.028	307.5	29.1	9.9	3.5	0.843	216.4	1.8	9.1	3.0		335.1	-48.9
BK2015_28_ChRM				295.0	-61.7																							
BK2015_29	MCU IVc	7	1.9	232.5	-67.8	71.8	7.2		7	3.63E-03	1.060	100.3	55.5	13.0	3.7	0.992	313.5	29.9	13.8	4.6	0.948	214.2	15.6	6.8	3.8		228.4	-67.6
BK2015_29_ChRM				254.6	-70.2																							
BK2015_30	MCU IVc, MCU IVd	6	2.0	321.9	-64.1	20.5	15.2		6	2.90E-02	1.185	116.3	55.4	17.3	2.0	0.978	278.6	33.3	19.5	4.7	0.837	14.1	8.3	17.9	2.6		331.1	-64.0
BK2015_31	MCU IVc	8	2.6	303.4	-64.3	180.9	4.1		8	4.95E-03	1.070	113.9	41.3	7.7	2.0	1.000	309.0	47.7	8.5	2.5	0.930	210.6	7.6	5.9	2.3		306.0	-65.7
BK2015_31_ChRM				293.2	-64.1																							
BK2015_32	MCU IVe'	11	6.9	10.0	-72.7	53.8	6.3		11	7.62E-02	1.193	286.2	67.8	8.0	3.3	0.962	55.9	14.6	9.7	4.6	0.845	150.3	16.3	9.7	7.3		353.5	-65.7
BK2015_40	MCU IIIc	8	1.2	243.5	-72.9	31.5	10.0		9	4.56E-03	1.066	85.6	47.9	24.6	11.0	0.998	311.1	32.3	24.3	13.9	0.936	204.9	23.8	16.7	7.9		241.7	-74.8
BK20*	MCU IVe'	6	9.6	69.4	-75.6	62.0	8.6		1	7.47E-02	not enough for statistics																NaN	NaN
BK34*	MCU IVe'	8	16.2	339.0	-81.3	238.0	3.6		7	8.08E-02	1.224	153.6	70.8	4.8	2.3	0.972	37.0	8.9	11.2	4.7	0.804	304.3	16.9	11.2	2.4		2.9	-85.6
BK38*	MCU IVe'	9	31.4	114.9	-85.5	37.0	8.6		9	6.99E-02	1.146	3.2	59.1	8.5	3.9	1.026	190.0	30.8	9.6	8.2	0.828	98.2	3.0	9.6	4.1		80.8	-85.0
BK42*	MCU IVe'	5	39.9	346.1	-79.7	579.0	3.2		3	5.54E-02	not enough for statistics																NaN	NaN
BK95*	MCU IVe'	5	7.2	223.4	-82.2	102.0	6.8		13	8.22E-02	1.183	118.4	58.2	8.4	3.9	0.940	212.7	2.7	21.8	4.1	0.877	304.4	31.7	21.8	8.2		175.0	-79.4
BK96*	MCU IVe'	6	9.9	183.4	-77.1	408.0	3.3		8	8.61E-02	1.189	290.6	63.0	4.8	2.8	0.953	38.5	8.9	5.9	4.7	0.859	132.7	25.2	6.0	2.8		212.2	-76.0
BK97*	MCU IVe'	7	14.4	320.1	-83.5	256.0	3.8		2	8.33E-02	not enough for statistics																NaN	NaN
BK98*	MCU IVe'	5	28.2	307.9	-78.7	186.0	6.6		4	1.20E-01	not enough for statistics																NaN	NaN
BK99*	MCU IVe'	5	29.3	271.0	-70.6	55.0	9.3		6	1.20E-01	1.247	347.5	34.8	5.7	3.1	0.975	93.3	21.3	6.8	4.2	0.778	208.5	47.4	7.7	2.5		300.5	-70.6
BK100*	MCU IVe'	6	19.7	263.8	-76.0	70.0	7.4		6	2.09E-02	1.106	339.1	66.6	4.7	3.9	1.027	195.0	19.3	7.2	3.5	0.866	100.5	12.7	7.0	3.0		272.0	-70.6
BK101*	MCU IVe'	4	55.0	11.0	-75.5	106.0	7.7		2	6.70E-02	not enough for statistics																NaN	NaN
BK104*	MCU IVe'	5	3.2	313.8	-59.1	399.0	3.4		12	8.87E-02	1.260	128.3	56.4	9.1	4.0	0.932	282.0	30.8	9.6	3.7	0.808	19.4	12.2	8.0	6.6		316.5	-59.8
BK105*	MCU IVe'	6	8.7	350.5	-58.9	108.0	5.9		5	1.08E-01	1.255	187.5	65.3	5.8	3.0	0.942	284.7	3.3	4.7	3.1	0.803	16.2	24.5	6.3	2.8		347.1	-55.7
BK107*	MCU IVe'	6	18.7	350.9	-76.4	97.0	6.3		10	9.70E-02	1.222	271.3	66.3	6.0	4.3	0.943	60.7	20.7	16.7	4.2	0.835	154.9	11.0	16.2	4.3		333.6	-68.6
BK112*	MCU IVe'	5	59.7	249.3	-79.1	203.0	5.4		5	8.68E-02	1.139	35.3	40.3	3.3	1.4	1.023	241.6	46.6	3.5	1.7	0.838	137.0	13.4	2.2	1.5		278.5	-78.7
BK113*	MCU IVe'	5	57.2	261.6	-80.5	85.0	8.3		7	7.45E-02	1.098	211.0	61.0	17.8	3.9	1.038	45.0	28.3	17.2	3.6	0.864	311.8	5.9	13.1	2.1		256.5	-79.3
BK114*	MCU IVe'	5	50.8	283.1	-60.5	60.0	9.9		6	6.45E-02	1.134	63.7	16.6	7.3	2.7	1.027	228.5	72.8	7.8	2.4	0.839	332.4	4.3	4.7	1.7		292.3	-59.9